https://doi.org/10.5194/egusphere-2024-3955
Preprint. Discussion started: 4 February 2025

Ice/firn age distribution on the Elbrus Western Plateau (Caucasus) inferred from ice flow model

Gleb Chernyakov[1], Nelly Elagina[1], Taisiia Kiseleva[1], and Stanislav Kutuzov[2, 3]

[1]Department of Glaciology, Institute of Geography, Russian Academy of Sciences, Moscow, Russia
[2]Byrd Polar and Climate Research Center, The Ohio State University, Columbus, OH, USA
[3]School of Earth Sciences, The Ohio State University, Columbus, OH, USA

Correspondence: Gleb Chernyakov (glchern@igras.ru)

Abstract. The glaciers of Mount Elbrus (Caucasus) contain paleoclimatic and paleoenvironmental information representative of a vast region. The cold conditions and negligible seasonal melting in the near-summit area of Elbrus ensure the excellent preservation of climatic signals. In 2009, a 182.65 meter long ice core was obtained from the Western Plateau (WP) of Elbrus at approximately 5100 m a.s.l. This core was partially dated using chemical stratigraphy (upper part) and radiocarbon dating (basal samples), serving as the basis for numerous paleoreconstructions. However, the ice age distribution within the intermediate part of the core and across the entire glacier on the WP remained unknown. In this work, a three-dimensional steady state full Stokes flow model for a cold glacier with a rheological law accounting for firn densification was applied both in a purely mechanical and in a thermomechanically coupled versions. Using this model, the ice velocity field was simulated in the central part of the WP. Ice age distribution was determined by solving a boundary value problem for the dating equation. All calculations were performed using Elmer/Ice, a finite element software designed for ice dynamics modeling. The model was calibrated by fitting the simulated age-depth relationship to the observed data from the ice core, with ice viscosity used as the primary calibration parameter. This approach provided a series of three-dimensional ice age distributions on the WP for various modeling scenarios. All versions of the model accurately reproduce the ice age according to ice core data to a depth of 140–150 m (130–180 years). Below 150 m, the ice age increases sharply and the dating discrepancies between different modeling scenarios become larger. Overall the modelled ages fell within 68.2 % confidence intervals of the radiocarbon dated near-bottom ice samples which indicated mean radiocarbon ages ranging from 1 to 2 ka. However, the model was unable to resolve the dating of the basal ice layer up to 3–4 m thick. Future model improvements should focus on refining basal conditions, including accounting for potential melting, and identifying areas containing the oldest ice.

1 Introduction

The glaciers of Mt. Elbrus offer a unique paleoclimate archive representative of a large region, including the North Caucasus, the Black Sea region, Southeastern Europe, North Africa, and the Middle East (Mikhalenko et al., 2024; Kutuzov et al., 2019a).

https://doi.org/10.5194/egusphere-2024-3955
Preprint. Discussion started: 4 February 2025

The cold conditions (10 m depth temperature of $-17.3\,^{\circ}\mathrm{C}$) and negligible seasonal melting in the near-summit region of Elbrus ensure the preservation of climatic and environmental signals in ice cores (Mikhalenko et al., 2015).

The Elbrus Western Plateau (WP) has been the subject of ice core studies since 2004 (Mikhalenko et al., 2005). Glaciochemical investigations of a deep ice core (182.65 m) drilled in 2009 include reconstructions of past anthropogenic sulfur emissions (Preunkert et al., 2019), black carbon (Lim et al., 2017), dust events (Kutuzov et al., 2013; Kutuzov et al., 2019a), ammonia (Legrand et al., 2024a), dissolved organic carbon (Legrand et al., 2024b), polycyclic aromatic hydrocarbons (Vecchiato et al., 2020), isotopic composition (Kozachek et al., 2017), and snow accumulation (Mikhalenko et al., 2024).

Relatively high annual accumulation (1.2 m w.e.) ensures the preservation of the seasonal cycle in geochemistry down to a depth of 168.6 m (131.6 m w.e.) in the ice core. This section was dated by annual layer counting, primarily using pronounced seasonal variations in ammonium and succinate concentrations (Preunkert et al., 2019). According to an estimate based on a two-dimensional (2D) analytical model (Salamatin et al., 2000), the age of the basal ice at the drilling site does not exceed 350–400 years, while the age of the deepest ice (more than 250 m deep) is about 660 years (Mikhalenko et al., 2015). Radiocarbon dating indicates that bottom ice samples from a depth of 176.89–182.15 m are between 1 and 2 ka old (Preunkert et al., 2019). Detailed ground-penetrating radar (GPR) surveys (Lavrentiev et al., 2010; Kutuzov et al., 2019b) revealed that the glacier ice at the WP site fills an ancient volcanic crater, resulting in specific morphological conditions (a large aspect ratio) and thermodynamic conditions (a high geothermal heat flux). More recently, the ice flow modeling was performed for the WP using a three-dimensional (3D) full Stokes ice flow model using only dynamical equations to account for the upstream effect in accumulation record (Mikhalenko et al., 2024). Despite significant progress in glaciological investigations of this site, several important questions remain unresolved, including the spatial ice age distribution.

The objectives of this study are to determine the spatial distribution of the ice/firn age at the WP and, in particular, to reconstruct the age of the intermediate section of the 2009 core, which had not previously been dated by other methods. We apply a thermomechanically coupled 3D flow model of the present-day glacier, based on the finite element modeling software Elmer/Ice (Gagliardini et al., 2013), which solves 3D full Stokes equations for a nonlinear viscous fluid with the firn rheological law (Gagliardini and Meyssonnier, 1997).

Ice flow models have been repeatedly used to study the age distribution of ice in mountain glaciers and, in particular, ice cores. 2D purely mechanical (Vincent et al., 1997) and thermomechanically coupled (Salamatin et al., 2000; Shiraiwa et al., 2001) analytical models were developed and applied for modeling age–depth relations in ice at Mt. Dôme du Goûter (Mont Blank, French Alps) and at Ushkovsky Volcano (Kamchatka Peninsula), respectively. (Gagliardini and Meyssonnier, 1997) adapted the rheological law of (Duva and Crow, 1994) for a cold glacier with a thick firn layer and implemented it in a 2D dynamical finite element model for Dôme du Goûter. Further, the firn rheological law of (Gagliardini and Meyssonnier, 1997) was applied in 2D and 3D finite element models for Colle Gnifetti glacier saddle (Monte Rosa, Swiss/Italian Alps) in the work (Lüthi and Funk, 2000). In (Zwinger et al., 2007) a 3D thermomechanically coupled full Stokes flow model with firn rheology for a crater glacier at Ushkovsky Volcano was implemented based on Elmer/Ice. (Konrad et al., 2013) used a semi-analytical 2D flow model with Glen's rheology in combination with the data of ice core and ground-penetrating radar for determining the age distribution of Colle Gnifetti. (Liciulli et al., 2020) applied a 3D full Stokes thermomechanically coupled model with

https://doi.org/10.5194/egusphere-2024-3955
Preprint. Discussion started: 4 February 2025

firn rheology implemented in Elmer/Ice to interpret ice core data at Colle Gnifetti and included this model to a more general transient simulation scheme.

2 Study area

The glacier area of Mt. Elbrus is around 112 km^2. Glaciers cover an altitudinal range from 2680 to 5642 m a.s.l. with the 0 °C) isotherm at around 5200 m a.s.l. Elbrus glaciers are currently losing mass (-0.55 ± 0.04 m w.e. a^{-1}). The rate of Elbrus glacier mass loss tripled in 1997–2017 compared with the 1957–1997 period (Kutuzov et al.,2019b). The ice cores used for climate and environment reconstructions were recovered at the WP at 5115 m a.s.l. (Mikhalenko et al., 2020). A 182.65 m ice core was recovered at the WP at a point with coordinates 43°20′53.9″ N and 42°25′36.0″ E in August–September 2009. The WP which covers approximately 0.5 km^2, is bordered by lava ridges to the south and southeast, and a vertical wall of Mount Elbrus to the east (Fig. 1). The results of a series of ground-based radar surveys at a frequency of 20 MHz in 2005, 2007, and 2017 show a significant ice thickness and a crater shape of the underlying bedrock. The maximum depth is 255 ± 8 m at the central part of the plateau, with minimum values of about 60 m near the edge. The 10 m depth temperature is -17.3 °C (Mikhalenko et al., 2015). A series of field measurement campaigns were conducted on the WP in 2004–2018, including the detailed low and high frequency GPR surveys, snow accumulation distribution measurements, meteorological measurements, snow pits and ice cores from several shallow and two deep (182.65 and 150 m) boreholes (Mikhalenko et al., 2020). For the information about topography, we used the Pléiades DEM with the vertical uncertainty between ± 0.5 m and ± 1 m (Kutuzov et al., 2019b). The Pléiades DEM used in this study was provided by the Pléiades Glacier Observatory initiative of the French Space Agency (CNES).

3 Research data

To model the flow and determine the age of ice/firn in the WP glacier, we used the following data:

1. Digital elevation models (DEMs) of the glacier surface and bedrock with a cell size of 10×10 m, obtained in 2017 based on radar surveys.
2. Temperature distribution in a deep-drilling borehole obtained from measurements in 2009.
3. Ice/firn density distribution in the 2009 deep ice core.
4. Ice/firn age distribution in the 2009 ice core with a resolution of about one year, obtained by laboratory methods (upper 168.6 m).
5. Interval age estimates of basal ice samples obtained by the radiocarbon method (lower 5.8 m).

https://doi.org/10.5194/egusphere-2024-3955
Preprint. Discussion started: 4 February 2025

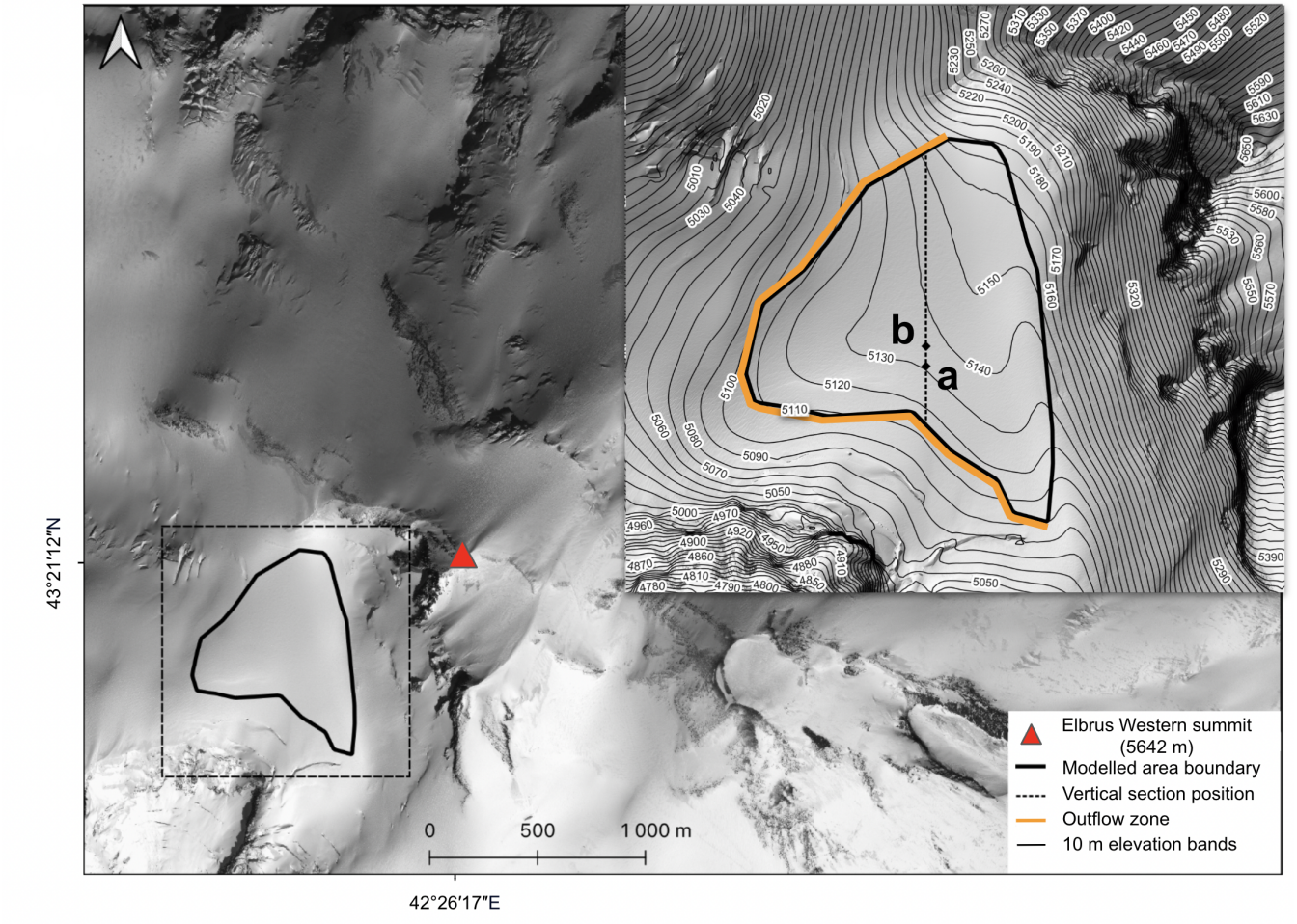

Figure 1. Study area on Mt. Elbrus. Geographic coordinates are presented in the WGS 84 (UTM 38 N). The SPOT 7 image obtained on 20 August 2016 is shown as a background. The elevation bands are based on the Pléiades DEM of 2017.

4 Spatial structure

Ice/firn flow modeling with subsequent dating was performed in a 3D domain (Fig. 2) covering a part of the glacier on the WP, for which DEMs (2017) of both the surface and the bed are available. The computational domain is limited by three surfaces: a part of the glacier surface; the lateral surface of the domain (the vertical "wall"); a part of the glacier base.

A flat computational grid (footprint) was created within the contour (shown in Fig. 1) of the area of the WP covered with DEMs. It contains 2508 nodes, 4734 linear triangular elements, and 280 linear one-dimensional elements on the boundary.

The volumetric computational grid was obtained by vertical extrusion of the flat grid. It is regular in the vertical direction (50 node levels) and characterized by a linear refinement of the step towards the glacier bed.

https://doi.org/10.5194/egusphere-2024-3955
Preprint. Discussion started: 4 February 2025

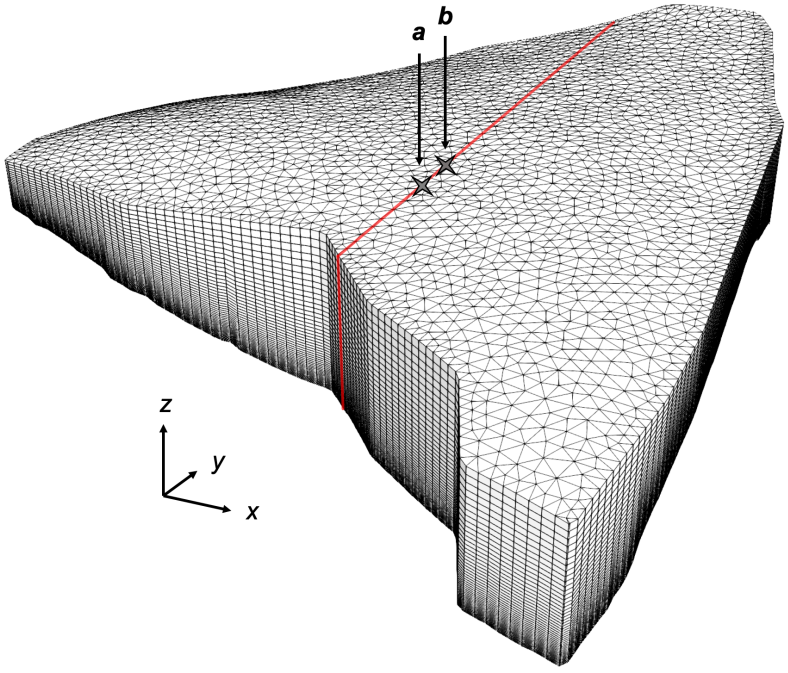

Figure 2. Computational domain and computational grid. The vertical distributions obtained in our study (Fig. 4) refer to location *a*; the 2009 drilling site is marked with *b*. The vertical section to which the simulation results presented in Fig. 3 relate is shown by the red line. Directions of coordinate axes: x – eastward, y – northward, z – upward.

According to DEMs ice thickness at the 2009 drilling site location is 6.1 m greater than ice core length. In our opinion, comparison of age–depth distributions (one modeled and one ice core based) for locations at a glacier with different ice thicknesses makes little sense. To represent the vertical profiles of ice/firn velocity, age and temperature and compare them with ice core data, we chose one of the points closest to the drilling site with similar ice thickness (182.67 m according to DEMs) and topography of surface and bedrock. This point (and corresponding vertical) is located 50 m south of the drilling site (denoted by *a* in Fig. 1, 2, and 3).

5 Mathematical model

The velocity distribution in the glacier allows one to calculate the time required for each ice/firn particle to move from the glacier surface to its current position. The calculation of the velocity field was performed on the basis of a 3D stationary full Stokes model with a rheological law for a compressible nonlinear viscous medium (ice/firn) (Gagliardini and Meyssonnier, 1997). We have applied both purely mechanical (isothermal) and thermomechanically coupled flow models. Information on the quantities used in the mathematical models is given in Table 1.

https://doi.org/10.5194/egusphere-2024-3955
Preprint. Discussion started: 4 February 2025

Table 1: Quantities. This table describes most of the quantities used in the mathematical model. The units in the table are chosen to be more representative, rather than coherent.

Group	Quantity	Description	Value / Dependent on	Units
Geometric	x, y	Horizontal coordinates	Independent variables	m
	z	Upward vertical coordinate	Independent variable	m
	s	Glacier surface altitude	x, y	m
	d	Depth	x, y, z	m
	H	Ice thickness	x, y	m
	$\boldsymbol{n}$	Outer unit normal vector to the computational domain boundary	x, y, z	–
Mechanical	ρ	Ice/firn density	d	$\mathrm{kg\,m^{-3}}$
	ρ_i	Pure ice density	918	$\mathrm{kg\,m^{-3}}$
	φ	Relative density	ρ	–
	p	Pressure	Free field	Pa
	$\boldsymbol{\sigma}$	Cauchy stress tensor	$p, \mu, \mathbf{D}$	Pa
	n	Stress exponent	3	–
	$\boldsymbol{v}$	Velocity	Free field	$\mathrm{m\,a^{-1}}$
	v_b	Basal normal velocity	10^{-6}	$\mathrm{m\,a^{-1}}$
	v_out	Lateral outflow velocity	d	$\mathrm{m\,a^{-1}}$
	v_max	Maximum lateral outflow velocity	20	$\mathrm{m\,a^{-1}}$
	$\mathbf{D}$	Strain-rate tensor	$\mathrm{grad}\,\boldsymbol{v}$	$\mathrm{a^{-1}}$
	$\boldsymbol{g}$	Gravitational acceleration	9.81	$\mathrm{m\,s^{-2}}$
	μ	Shear viscosity	T', δ, φ	$\mathrm{Pa\,s}$
	E	Flow enhancement factor	$0.016, 0.2, 0.25$	–
Thermodynamic	T	Temperature	Free field	K
	T_m	Melting temperature of ice	p	K
	T_0	Melting temperature of ice for low pressure	273.15	K
	T'	Temperature relative to the pressure melting point	p, T	K
	T_s	Glacier surface temperature	-18	°C
	β	Clausius-Clapeyron constant for air-saturated ice	9.8×10^{-8}	$\mathrm{K\,Pa^{-1}}$
	A	Rate factor	2.291×10^{-25} / T'	$\mathrm{Pa^{-3}\,s^{-1}}$

https://doi.org/10.5194/egusphere-2024-3955
Preprint. Discussion started: 4 February 2025

	A_0	Pre-exponential constant	$\begin{cases} 3.985 \times 10^{-13} & (T' \leq 263.15\,\mathrm{K}) \\ 1.916 \times 10^{3} & (T' > 263.15\,\mathrm{K}) \end{cases}$	$\mathrm{Pa^{-3}\,s^{-1}}$
	Q	Activation energy	$\begin{cases} 60 & (T' \leq 263.15\,\mathrm{K}) \\ 139 & (T' > 263.15\,\mathrm{K}) \end{cases}$	$\mathrm{kJ\,mol^{-1}}$
	R	Universal gas constant	8.314	$\mathrm{J\,mol^{-1}\,K^{-1}}$
	c	Specific heat	T	$\mathrm{J\,kg^{-1}\,K^{-1}}$
	κ	Heat conductivity	T	$\mathrm{W\,m^{-1}\,K^{-1}}$
	$\boldsymbol{q}$	Heat flux	$T, \mathrm{grad}\,T$	$\mathrm{W\,m^{-2}}$
	q_{geo}	Geothermal flux	0.34	$\mathrm{W\,m^{-2}}$
Other	t	Time	Independent variable	a
	$\mathcal{A}$	Ice/firn age	Free field	a
	δ	Tensor invariant	$\mathbf{D}, \varphi$	$\mathrm{s^{-1}}$
	a, b	Flow law auxiliary functions	φ	–

5.1 Dating problem

In order to obtain a 3D age field of ice/firn $\mathcal{A}(x,y,z)$, we first calculated the velocity field $\boldsymbol{v}(x,y,z)$ in the computational domain and then solved the dating equation $\mathrm{d}\mathcal{A}/\mathrm{d}t = 1$, or

$$\frac{\partial \mathcal{A}}{\partial t} + \boldsymbol{v} \cdot \mathrm{grad}\,\mathcal{A} = 1 \tag{1}$$

with a boundary condition of zero age at the surface of the glacier:

$$\mathcal{A}|_{\mathrm{s}} = 0. \tag{2}$$

Due to the steady-state assumption $\partial\mathcal{A}/\partial t \equiv 0$.

5.2 Constitutive relations

The velocity field calculation for the WP glacier was performed based on a 3D steady-state full Stokes flow model with rheological law (Gagliardini and Meyssonnier, 1997) for a compressible nonlinear-viscous medium (ice/firn). The mathematical formulation of the ice/firn flow problem with some modifications follows (Zwinger et al., 2007).

Next, the constitutive equations of the model are subsequently introduced. Based on the surface heights, a depth field is calculated in the entire 3D domain:

$$d(x,y,z) = s(x,y) - z. \tag{3}$$

https://doi.org/10.5194/egusphere-2024-3955
Preprint. Discussion started: 4 February 2025

Based on an approximation of the density distribution in the 2009 ice core, the ice/firn density in the glacier is represented as a function of depth as follows:

$$\rho(d) = \begin{cases} \rho_{\mathrm{i}}\left(1 - 0.56e^{-0.028d}\right), & d < 104.5\ \mathrm{m} \\ 0.97\rho_{\mathrm{i}}, & d \geq 104.5\ \mathrm{m}. \end{cases} \tag{4}$$

The functions of the relative density φ ($\varphi = \rho/\rho_{\mathrm{i}}$)

$$a(\varphi) = \begin{cases} \exp\left(13.2224 - 15.78652\varphi\right), & \varphi \leq 0.81 \\ \frac{1}{3}\left(5 - 2\varphi\right)\varphi^{-\frac{2n}{n+1}}, & \varphi > 0.81 \end{cases} \tag{5}$$

and

$$b(\varphi) = \begin{cases} \exp\left(15.09371 - 20.46489\varphi\right), & \varphi \leq 0.81 \\ \frac{3}{4}\left(\frac{(1-\varphi)^{\frac{1}{n}}}{n\left(1-(1-\varphi)^{\frac{1}{n}}\right)}\right)^{\frac{2n}{n+1}}, & \varphi > 0.81 \end{cases} \tag{6}$$

are used to construct the flow law relations in accordance with (Gagliardini and Meyssonnier, 1997).

The strain-rate tensor is a symmetric part of the velocity gradient:

$$\mathbf{D} = \frac{1}{2}\left(\operatorname{grad}\boldsymbol{v} + (\operatorname{grad}\boldsymbol{v})^{\mathrm{T}}\right). \tag{7}$$

Decomposing the strain-rate tensor into an isotropic and a deviatoric parts, we obtain:

$$\mathbf{D} = \frac{\operatorname{div}\boldsymbol{v}}{3}\mathbf{I} + \mathbf{D}^{\mathrm{D}}. \tag{8}$$

Hereinafter the superscripts T and D denote the transpose and the deviator of a tensor, respectively; I is the unit tensor. The first invariant of the strain-rate tensor is represented in the form of the velocity divergence.

Following (Gagliardini and Meyssonnier, 1997), we introduce the tensor invariant

$$\delta = \sqrt{\frac{2\operatorname{tr}\left(\mathbf{D}^{\mathrm{D}}\right)^2}{a(\varphi)} + \frac{(\operatorname{div}\boldsymbol{v})^2}{b(\varphi)}}, \tag{9}$$

where tr denotes the trace of a tensor.

The melting temperature of ice is considered to be pressure-dependent: $T_{\mathrm{m}} = T_0 - \beta p$. The temperature relative to the pressure melting point is defined as follows: $T' = T - T_{\mathrm{m}} + T_0$ (Greve and Blatter, 2009).

In the case of thermomechanically coupled model, the rate factor A is dependent on the temperature relative to the pressure melting point T' and is determined by the Arrhenius law:

$$A(T') = A_0 e^{-\frac{Q}{RT'}}. \tag{10}$$

https://doi.org/10.5194/egusphere-2024-3955
Preprint. Discussion started: 4 February 2025

Then the viscosity of ice/firn can be expressed as follows:

$$\mu(T', \delta, \varphi) = \frac{(2EA(T'))^{-\frac{1}{n}} \delta^{\frac{1-n}{n}}}{a(\varphi)}. \tag{11}$$

The constant flow enhancement factor E in Eq. (11) is used as a calibration parameter.

After splitting Cauchy stress tensor into an isotropic and a deviatoric part

$$\boldsymbol{\sigma} = -p\mathbf{I} + \boldsymbol{\sigma}^{\mathrm{D}} \tag{12}$$

we can write the rheological law in general form:

$$\boldsymbol{\sigma}^{\mathrm{D}} = 2\mu\mathbf{D}^{\mathrm{D}}. \tag{13}$$

The specific heat

$$c(T) = 146.3 + 7.253T \tag{14}$$

and the heat conductivity

$$\kappa(T) = 9.828e^{-0.0057T} \tag{15}$$

of the ice/firn are temperature-dependent.

The heat flux is determined by Fourier's law of heat conduction:

$$\boldsymbol{q} = -\kappa \operatorname{grad} T. \tag{16}$$

5.3 Field equations

The mechanical field equations of the model are the volume balance equation

$$\operatorname{div} \boldsymbol{v} + \frac{b(\varphi)}{a(\varphi)\mu} p = 0 \tag{17}$$

and the Stokes equation

$$\operatorname{div} \boldsymbol{\sigma} + \rho \boldsymbol{g} = \mathbf{0}. \tag{18}$$

In the case of thermomechanically coupled model the mechanical equations are supplemented with the heat transfer equation

$$\rho c \left(\frac{\partial T}{\partial t} + \boldsymbol{v} \cdot \operatorname{grad} T \right) = -\operatorname{div} \boldsymbol{q} + \operatorname{tr}(\boldsymbol{\sigma} \cdot \mathbf{D}), \quad T \leq T_{\mathrm{m}}. \tag{19}$$

Since the model is steady-state, $\partial T / \partial t \equiv 0$. The solution is limited by the pressure melting point T_{m}.

https://doi.org/10.5194/egusphere-2024-3955
Preprint. Discussion started: 4 February 2025

5.4 Boundary conditions

Boundary conditions (BCs) are specified separately at three areas of the boundary of the computational domain: the surface, the base, and the lateral side.

5.4.1 Surface boundary conditions

Surface BCs apply to the part of the glacier surface under consideration (designated by the subscript s). They include the stress-free condition

$$(\boldsymbol{\sigma} \cdot \boldsymbol{n})|_{\mathrm{s}} = \mathbf{0} \tag{20}$$

and the surface temperature condition

$$T|_{\mathrm{s}} = T_{\mathrm{s}}. \tag{21}$$

The surface temperature value $T_{\mathrm{s}} = -18\ ^{\circ}\mathrm{C}$ is selected on the basis of 2009 borehole temperature measurements ($-17\ ^{\circ}\mathrm{C}$ at 10 m depth) and meteorologically based estimation of the annual mean air temperature at the drill site of $-19\ ^{\circ}\mathrm{C}$ (Mikhalenko et al., 2015).

5.4.2 Basal boundary conditions

Basal BCs (denoted by b) apply to the bedrock of the glacier. The dynamical basal BC implies a cold base (zero tangential velocity) and a small normal outflow ice velocity at the bedrock:

$$\boldsymbol{v}|_{\mathrm{b}} = v_{\mathrm{b}} \boldsymbol{n}|_{\mathrm{b}}\,. \tag{22}$$

The constant geothermal flux is specified as the thermodynamic bedrock BC:

$$(\kappa \operatorname{grad} T \cdot \boldsymbol{n})|_{\mathrm{b}} = q_{\mathrm{geo}}. \tag{23}$$

The value of the basal heat flux $q_{\mathrm{geo}} = 0.34\ \mathrm{W\,m^{-2}}$ was calculated from the temperature measurements near the bottom of the 2009 borehole (Mikhalenko et al., 2015).

5.4.3 Lateral boundary conditions

Lateral BCs (denotation l) are specified at the vertical surface surrounding the modeled area and connecting the upper and lower parts of the computational domain boundary (glacier surface and bedrock). When modeling lateral outflow, the lateral BCs differ at the eastern (l, E) and western (l, W) sides of the domain, since the outflow is applied only at the western side (Fig. 1).

The WP glacier is bounded on the east by a steep wall of Elbrus summit, so we assume that there is no outflow from the domain through the eastern boundary:

$$(\boldsymbol{v} \cdot \boldsymbol{n})|_{\mathrm{l,\,E}} = 0. \tag{24}$$

https://doi.org/10.5194/egusphere-2024-3955
Preprint. Discussion started: 4 February 2025

The western side of the plateau is characterized by westward slope, so outflow is expected at the western boundary of the domain. During field work, measurements of ice velocity on the glacier surface were not carried out. In this regard, we have performed all simulations for two extreme cases: 1) the outflow through the lateral side of the domain is completely absent; 2) the outflow is faster (20 $\mathrm{m\,a^{-1}}$ at the western rim of the surface) than would be expected in real conditions:

$$(\boldsymbol{v}\cdot\boldsymbol{n})|_{\mathrm{l,W}} = 0 \quad \text{or} \quad (\boldsymbol{v}\cdot\boldsymbol{n})|_{\mathrm{l,W}} = v_{\mathrm{out}}, \tag{25}$$

where

$$v_{\mathrm{out}}(d) = v_{\mathrm{max}}\left(1 - \left(\frac{d}{H}\right)^4\right). \tag{26}$$

Here we assume that horizontal outflow decreases with depth in accordance with the forth power law. Similar relations are discussed in literature, e.g. (Hooke, 2019; Greve and Blatter, 2009).

Zero normal heat flux is assumed at the entire lateral boundary:

$$(\kappa \operatorname{grad} T\cdot\boldsymbol{n})|_{\mathrm{l}} = 0. \tag{27}$$

The differential equations of Sect. 5.3 together with the material equations of Sect. 5.2 and the boundary conditions of Sect. 5.4 form a complete boundary value problem for determining the unknown fields $\boldsymbol{v}$, p, and T.

5.5 Reduced model

All the simulation variants produced on the basis of the thermomechanically coupled model were also repeated by means of a purely mechanical model, i.e. a reduced flow model with the heat transfer block switched off.

The reduction of the complete model is as follows. The ice/firn temperature is assumed to be constant ($-14\ ^\circ\mathrm{C}$) and close to the average value inferred from borehole measurements in 2009. In this case, the rate factor is constant (2.291×10^{-25} $\mathrm{Pa^{-3}\,s^{-1}}$) and corresponds to this temperature (Cuffey and Paterson, 2010). Hence, the viscosity lacks the dependency on temperature and pressure (see Eq. (11)).

6 Numerical methods

All simulations were performed numerically based on the finite element method in the framework of dedicated ice flow modeling software Elmer/Ice (Gagliardini et al., 2013).

In Elmer/Ice differential field equations are solved numerically via their transformation to a discretized variational form (Gagliardini et al., 2013). Since our initial differential problem is nonlinear, the discretized equations of its variational (weak) formulation are also nonlinear and need to be solved iteratively.

For the thermomechanically coupled model there is a nonlinear iteration loop between the Stokes equation (18) (together with the volume balance equation (17)) and the heat transfer equation (19). On each step of the nonlinear iteration a system of linear algebraic equations arise and need to be solved both for the Stokes equation and for the heat transfer equation. The linear

https://doi.org/10.5194/egusphere-2024-3955
Preprint. Discussion started: 4 February 2025

systems for the Stokes equations are solved via an iterative method – the biconjugate gradient stabilized method (BiCGStab) whith zero-fill incomplete lower–upper preconditioner (ILU(0)). The linear systems for the heat transfer equation are solved via a direct method - unsymmetric-pattern multifrontal method, implemented in the solver UMFPACK.

In a purely mechanical case linear algebraic systems for the Stokes equation are solved via the same iterative method and preconditioner as in the coupled model.

The dating equation (1) is solved in a final step based on a precalculated velocity field. The equation was discretized via discontinuous Galerkin method and the resulting linear algebraic systems were solved by a direct method for the thermomechanically coupled model and by BiCGStab with ILU(1) preconditioner for the purely mechanical model.

7 Model calibration

In order to provide the best fit between age–depth distributions simulated for the location *a* and derived from empirical data for the location *b* (Fig. 1), we varied three independent characteristics of the model. The first is the general type of the model (thermomechanically coupled or purely mechanical). The second is the presence or absence of lateral ice/firn outflow. The third characteristic is the viscosity value; its tuning is what constitutes the calibration procedure. Technically, the calibration of viscosity comes down to choice of the value of flow enhancement factor.

8 Results

The results presented below correspond to three selected simulation cases among numerous cases for each of which the ice-core-derived age–depth dependency is reproduced relatively well. These cases represent limiting scenarios, as the age–depth curves for the remaining simulations lie within the region bounded by the curves of these three cases. The combinations of model characteristics for these cases are presented in Table 2.

Figure 3 illustrates the simulation results for a purely mechanical model without lateral outflow, showing the velocity magnitude and isochrones in the vertical section passing through the 2009 drilling site. Figure 4 presents vertical profiles of modeled velocity, age, and temperature of the ice/firn at a selected location shifted slightly southward from the drilling site. The modeling results are compared to the laboratory-derived 2009 ice core dating results (Fig. 4b) and the borehole temperature measurements from 2009 (Fig. 4c).

In Figure 4b, the dating of the upper 168.6 m section of the ice core (Mikhalenko et al., 2024) is referred to as "Measured data". This is a revised version of the chronology by Preunkert et al. (2019), dating the deepest layers back to 1750. Additionally, calibrated date ranges at a 68.2 % confidence level for radiocarbon dating (Preunkert et al., 2019) of four basal ice samples are shown. The depth ranges of the sampled ice are 177.11 $\pm$ 0.22 m, 179.19 $\pm$ 0.14 m, 181.50 $\pm$ 0.13 m, and 182.02 $\pm$ 0.13 m (Preunkert et al., 2019).

https://doi.org/10.5194/egusphere-2024-3955
Preprint. Discussion started: 4 February 2025

Table 2. Comparison of datings of reference horizons.

E	0.016	0.2	0.25		
Lateral outflow	No	Yes	No		
Model type	Thermomechanical	Mechanical	Mechanical		
d (m)	Model date (CE)			Proxy date (CE)	Proxy description
75.6	1959	1966	1979	1963	^{3}H
116.7	1920	1913	1945	1912	Katmai
146.38	1866	1829	1886	1854	Shiveluch
153.7	1838	1785	1853	1815	Tambora
154.73	1831	1774	1845	1815	Tambora
160.4	1807	1734	1815	1783	Laki
177.11	1367	981	1288	670–1245	^{14}C
179.19	1021	386	877	130–770	^{14}C

https://doi.org/10.5194/egusphere-2024-3955
Preprint. Discussion started: 4 February 2025

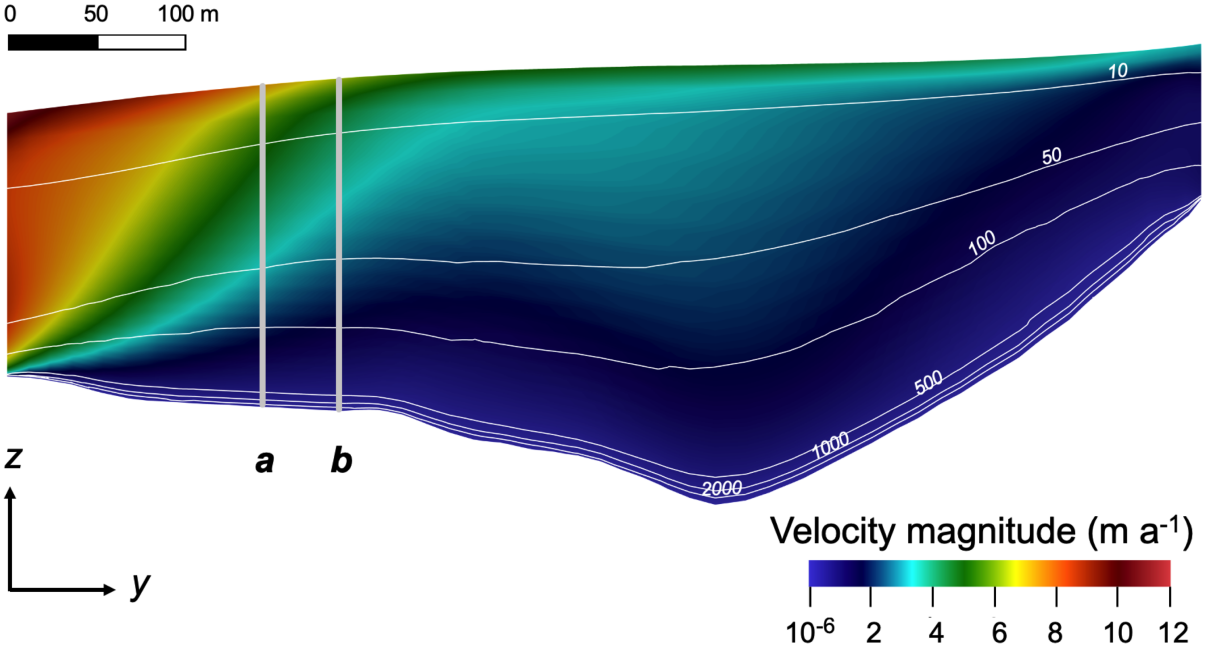

Figure 3. Cross-section of the computational domain by a vertical plane (case $E = 0.25$, $v_{\text{out}} = 0$). The cross-section is drawn in the north-south direction and passes through the drilling site of 2009 (vertical *b*; the modeling results presented in Fig. 4 refer to vertical *a*). The y coordinate axis is directed north, z – upwards. The colors of the rainbow show the velocity value (m/a). The white curves are isochrones corresponding to the model ice/firn ages of 10, 50, 100, 500, 1000, and 2000 years.

https://doi.org/10.5194/egusphere-2024-3955
Preprint. Discussion started: 4 February 2025

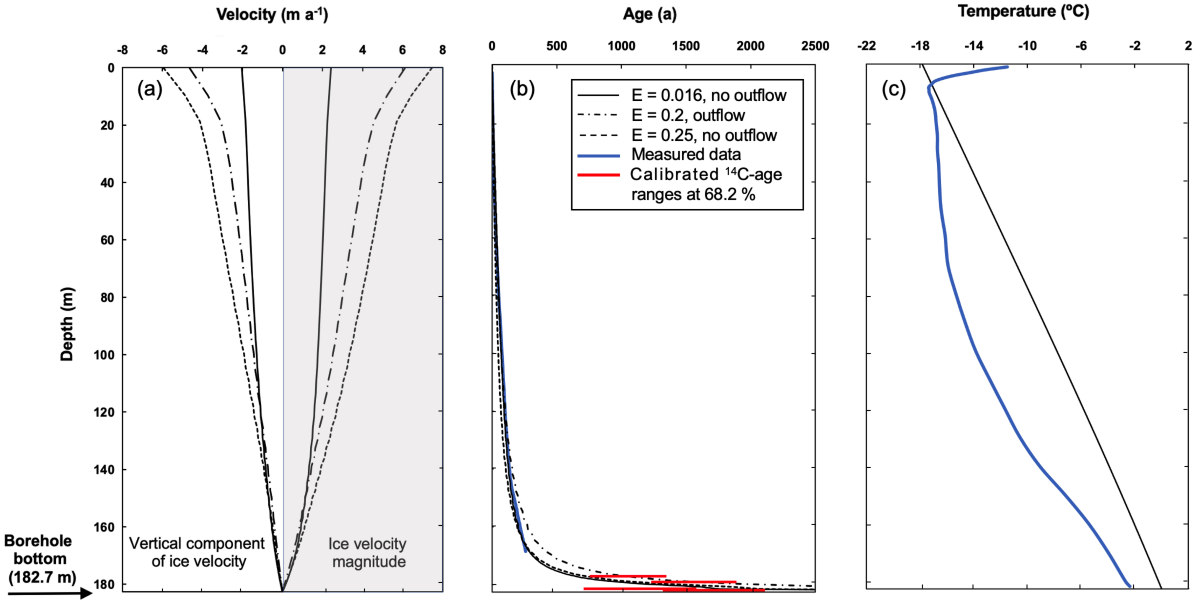

Figure 4. Modeled ice/firn velocity (a), age (b), and temperature (c) profiles for vertical *a* (see Fig. 3) and empirical data.

Table 2 compares the dates obtained from our simulations with the 2009 ice core dating for reference horizons and the two upper basal ice samples. Similar to the vertical profiles in Fig. 4, these model results correspond to location *a* rather than the drilling site *b* (Fig. 1). The depth values for the tritium horizon (^{3}H), formed as a result of nuclear tests, and for volcanic horizons (Katmai, Shiveluch, Tambora, and Laki) provided based on the more reliable of the two main chronologies in (Mikhalenko et al., 2024). Notably, Table 2 also reflects the uncertainty in determining the depth of the Tambora volcanic layer. For the bottom ice samples, the table presents the median sample depths along with calibrated ^{14}C date ranges at a 68.2 % confidence level, as reported by Preunkert et al. (2019).

9 Discussion

Due to incomplete data, the modeling of the velocity field and ice age of the WP glacier was conducted under several simplifying assumptions and limitations. The key assumptions are as follows:

1. *Stationarity:* This assumes a steady-state geometry of the glacier, along with unchanging density, velocity, pressure, and temperature fields.

2. *Lack of velocity data:* No direct measurements of the glacier's velocity field are available.

https://doi.org/10.5194/egusphere-2024-3955
Preprint. Discussion started: 4 February 2025

3. *Surface temperature boundary condition:* The temperature at the glacier surface reflects early 21st-century conditions and does not account for historical variations.
4. *Geothermal flux:* A locally determined geothermal flux value is extrapolated across the entire glacier bed.
5. *No basal melting:* The model does not incorporate the potential effects of basal melting.
6. *Ice thickness uncertainty:* Ice thickness estimates have an uncertainty of several meters.
7. *Spatial mismatch:* The simulations performed for a site that does not match exactly the location of the 2009 drilling site.

Conditions 1–4 are determined by the lack of data on the modern and historical state of glaciation of the WP. Concerning condition 5, a study of the WP temperature regime (Mikhalenko et al., 2015), based on the method proposed by Salamatin et al. (2001), suggested basal melting occurs at depths exceeding 220 m, with rates not exceeding 10 mm water equivalent per year. Condition 7 is a consequence of condition 6.

The positioning of isochrones (Fig. 3) indicates minimal differences in the ice/firn age distributions between verticals *a* and *b*. Thus, using the age distribution from vertical *a* for model calibration gives a satisfactory representation of the broader area, including the 2009 core drilling site.

As highlighted, the region between the curves in Fig. 4b represents the range of age-depth relationships derived from the modeling, as these curves correspond to the limiting cases. From this perspective, the model accurately reproduces the ice age for the upper part of the core (down to a depth of 140–150 m), overestimates the age in the depth range of 150–170 m, and aligns with the 68.2 % confidence intervals for the ages of the upper two of the four basal ice samples. However, steady-state models for cold glaciers are known to be unsuitable for dating the deepest ice layers near the bedrock (Zwinger et al., 2007).). Consequently, our model could not capture the age confidence intervals for the two lowermost basal ice samples (Fig. 4b).

The vertical temperature distribution, simulated using the thermomechanically coupled model, qualitatively reflects observed trends but shows a tendency toward overestimation (Fig. 4c).

10 Conclusions

Based on the simulation of glacier dynamics, a 3D ice/firn age distribution in the glacier on the Elbrus Western Plateau was obtained. The pattern of isochronous surfaces suggests that the obtained ice ages are generally representative of the area near the 2009 drilling site. The dating results are robust to small variations in the calibrated model parameters and align closely with the dating of the upper part of the 2009 ice core. In two of the three model cases, the correspondence extends to a depth of 165 m (1766 CE according to the core). In the depth range 3.3–5.8 m above the bedrock, all model dates (320–1389 CE) fall within or near the 68.2 % confidence intervals of radiocarbon-dated ice core samples. Comparison with ice core data supports the validity of the model dating except for the 3–4 m bottom layer. Additionally, the model provided an approximate reconstruction of the previously undated middle part of the 2009 ice core.

https://doi.org/10.5194/egusphere-2024-3955
Preprint. Discussion started: 4 February 2025

Data availability. Input data for Elbrus Western Plateau (Caucasus) ice flow model are available at https://doi.org/10.5281/zenodo.14795959 (Chernyakov et al., 2025).

Author contributions. GC performed the simulations and prepared the manuscript with contributions from all co-authors, NE performed visualization of the data and results, TK provided the study area description and mapping, SK contributed to conceptualization and writing.

Competing interests. The authors declare that they have no conflict of interest.

Acknowledgements. The work of Gleb Chernyakov, Nelly Elagina, and Taisiia Kiseleva was carried out within the framework of the Russian Science Foundation project no. 24-27-00262. We thank Olivier Gagliardini and Vladimir Mikhalenko for fruitful discussions that significantly contributed to the work.

https://doi.org/10.5194/egusphere-2024-3955
Preprint. Discussion started: 4 February 2025

References

Chernyakov, G., Kutuzov, S., Lavrentiev, I., Mikhalenko, V.: Input data for Elbrus Western Plateau (Caucasus) ice flow model, Zenodo [data set], https://doi.org/10.5281/zenodo.14795959, 2025.

Cuffey, K. M. and Paterson, W. S. B.: The physics of glaciers, Academic Press, 2010.

Duva, J. M. and Crow, P. D.: Analysis of consolidation of reinforced materials by power-law creep, Mech. Mater., 17, 25–32, 1994.

Gagliardini, O. and Meyssonnier, J.: Flow simulation of a firn-covered cold glacier, Ann. Glaciol., 24, 242–248, https://doi.org/10.3189/S0260305500012246, 1997.

Gagliardini, O., Zwinger, T., Gillet-Chaulet, F., Durand, G., Favier, L., De Fleurian, B., Greve, R., Malinen, M., Martín, C., Räback, P., Ruokolainen, J., Sacchettini, M., Schäfer, M., Seddik, H., and Thies, J.: Capabilities and performance of Elmer/Ice, a new-generation ice sheet model, Geosci. Model Dev., 6, 1299–1318, https://doi.org/10.5194/gmd-6-1299-2013, 2013.

Greve, R. and Blatter, H.: Dynamics of Ice Sheets and Glaciers, Springer, Berlin, Germany, 2009.

Hooke, R. L. B.: Principles of Glacier Mechanics, 3rd ed., Cambridge University Press, 2019.

Konrad, H., Bohleber, P., Wagenbach, D., Vincent, C., and Eisen, O.: Determining the age distribution of Colle Gnifetti, Monte Rosa, Swiss Alps, by combining ice cores, ground-penetrating radar and a simple flow model, J. Glaciol., 59, 179–189, https://doi.org/10.3189/2013JoG12J072, 2013.

Kozachek, A., Mikhalenko, V., Masson-Delmotte, V., Ekaykin, A., Ginot, P., Kutuzov, S., Legrand, M., Lipenkov, V., and Preunkert, S.: Large-scale drivers of Caucasus climate variability in meteorological records and Mt El'brus ice cores, Clim. Past, 13, 473–489, https://doi.org/10.5194/cp-13-473-2017, 2017.

Kutuzov, S., Shahgedanova, M., Mikhalenko, V., Ginot, P., Lavrentiev, I., and Kemp, S.: High-resolution provenance of desert dust deposited on Mt. Elbrus, Caucasus in 2009–2012 using snow pit and firn core records, Cryosphere, 7, 1481–1498, https://doi.org/10.5194/tc-7-1481-2013, 2013.

Kutuzov, S., Legrand, M., Preunkert, S., Ginot, P., Mikhalenko, V., Shukurov, K., Poliukhov, A., and Toropov, P.: The Elbrus (Caucasus, Russia) ice core record-Part 2: History of desert dust deposition, Atmos. Chem. Phys., 19, 14133–14148, https://doi.org/10.5194/acp-19-14133-2019, 2019a.

Kutuzov, S., Lavrentiev, I., Smirnov, A., Nosenko, G., and Petrakov, D.: Volume Changes of Elbrus Glaciers From 1997 to 2017, Front. Earth Sci., 7, https://doi.org/10.3389/feart.2019.00153, 2019b.

Lavrentiev, I. I., Mikhalenko, V. N., and Kutuzov, S. S.: Ice thickness and subglacial relief of the Western ice plateau of Elbrus [in Russian], Ice and Snow, 2, 2–18, 2010.

Legrand, M., Vorobyev, M., Bokuchava, D., Kutuzov, S., Plach, A., Stohl, A., Khairedinova, A., Mikhalenko, V., Vinogradova, M., Eckhardt, S., and Preunkert, S.: Measurement Report: Changes of ammonia emissions since the 18th century in south-eastern Europe inferred from an Elbrus (Caucasus, Russia) ice core record, EGUsphere [preprint], https://doi.org/10.5194/egusphere-2024-1381, 2024a.

Legrand, M., Preunkert, S., Kutuzov, S., Siour, G., Mikhalenko, V., Dolgova, E., and Friedrich, R.: 20th Century changes of DOC and its 14C signature archived in Caucasus ice-core: Implications for past sources of organic carbon aerosol in south-eastern Europe. Journal of Geophysical Research: Atmospheres, 129, e2023JD040121, https://doi.org/10.1029/2023JD04012, 2024b.

Licciulli, C., Bohleber, P., Lier, J., Gagliardini, O., Hoelzle, M., and Eisen, O.: A full Stokes ice-flow model to assist the interpretation of millennial-scale ice cores at the high-Alpine drilling site Colle Gnifetti, Swiss/Italian Alps, J. Glaciol., 66, 35–48, https://doi.org/10.1017/jog.2019.82, 2019.

https://doi.org/10.5194/egusphere-2024-3955
Preprint. Discussion started: 4 February 2025

Lim, S., Faïn, X., Ginot, P., Mikhalenko, V., Kutuzov, S., Paris, J. D., Kozachek, A., and Laj, P.: Black carbon variability since preindustrial times in the eastern part of Europe reconstructed from Mt. Elbrus, Caucasus, ice cores, Atmos. Chem. Phys., 17, 3489–3505, https://doi.org/10.5194/acp-17-3489-2017, 2017.

Lüthi, M. and Funk, M.: Dating of ice cores from a high Alpine glacier with a flow model for cold firn, Ann. Glaciol., 31, 69–79, https://doi.org/10. 3189/172756400781820381, 2000.

Mikhalenko, V., Sokratov, S., Kutuzov, S., Ginot, P., Legrand, M., Preunkert, S., Lavrentiev, I., Kozachek, A., Ekaykin, A., Faïn, X., Lim, S., Schotterer, U., Lipenkov, V., and Toropov, P.: Investigation of a deep ice core from the Elbrus western plateau, the Caucasus, Russia, Cryosph., 9, 2253–2270, https://doi.org/10.5194/tc-9-2253-2015, 2015.

Mikhalenko, V., Kutuzov, S., Toropov, P., Legrand, M., Sokratov, S., Chernyakov, G., Lavrentiev, I., Preunkert, S., Kozachek, A., Vorobiev, M., Khairedinova, A., and Lipenkov, V.: Accumulation rates over the past 260 years archived in Elbrus ice core, Caucasus, Clim. Past, 20, 237–255, https://doi.org/10.5194/cp-20-237-2024, 2024.

Mikhalenko, V. N., Kutuzov, S. S., Lavrentiev, I. I., Kunakhovich, M. G., and Thomson, L. G.: Western Elbrus Plateau studies: results and perspectives [in Russian], Mater. Glyatsiologicheskikh Issled. Data Glaciol. Stud., 99, 185–190, 2005.

Mikhalenko, V. N. (Ed.): Elbrus Glaciers and Climate, Nestor-Historia Publications, Moscow-St. Petersburg, Russia, ISBN 978-5-4469-1671-9, 2020.

Preunkert, S., Legrand, M., Kutuzov, S., Ginot, P., Mikhalenko, V., and Friedrich, R.: The Elbrus (Caucasus, Russia) ice core record – Part 1: reconstruction of past anthropogenic sulfur emissions in south-eastern Europe, Atmos. Chem. Phys., 19, 14119–14132, https://doi.org/10.5194/acp-19-14119-2019, 2019.

Salamatin, A. N., Murav'yev, Y. D., Shiraiwa, T., and Matsuoka, K.: Modelling dynamics of glaciers in volcanic craters, J. Glaciol., 46, 177–187, 2000.

Salamatin, A. N., Shiraiwa, T., Muravyev, Y. D., Kameda, T., Silantiyeva, E., and Ziganshin, M.: Dynamics and borehole temperature memory of Gorshkov Ice Cap on the summit of Ushkovsky Volcano, Kamchtka Peninsula, in: Proceedings of the International Symposium on the Atmosphere–Ocean–Cryosphere Interaction in the Sea of Okhotsk and the Surrounding Environments held at Institute of Low Temperature Science, Hokkaido University, Sapporo, Japan, 12–15 December 2000, 120–121, 2001.

Shiraiwa, T., Muravyev, Y. D., Kameda, T., Nishio, F., Toyama, Y., Takahashi, A., Ovsyannikov, A. A., Salamatin, A. N., and Yamagata, K.: Characteristics of a crater glacier at Ushkovsky volcano, Kamchatka, Russia, as revealed by the physical properties of ice cores and borehole thermometry, J. Glaciol., 47, 423–432, https://doi.org/10.3189/172756501781832061, 2001.

Vecchiato, M., Gambaro, A., Kehrwald, N. M., Ginot, P., Kutuzov, S., Mikhalenko, V., and Barbante, C.: The Great Acceleration of fragrances and PAHs archived in an ice core from Elbrus, Caucasus, Sci. Rep., 10, 1–10, https://doi.org/10.1038/s41598-020-67642-x, 2020.

Vincent, C., Vallon, M., Pinglot, J. F., Funk, M., and Reynaud, L.: Snow accumulation and ice flow at Dôme du Goûter (4300 m), Mont Blanc, French Alps, J. Glaciol., 43, 513–521, https://doi.org/10.3189/S0022143000035127, 1997.

Zwinger, T., Greve, R., Gagliardini, O., Shiraiwa, T., and Lyly, M.: A full Stokes-flow thermo-mechanical model for firn and ice applied to the Gorshkov crater glacier, Kamchatka, Ann. Glaciol., 45, 29–37, https://doi.org/10.3189/172756407782282543, 2007.